Quantitative imaging of a non-combusting diesel spray using structured laser illumination planar imaging

Berrocal, Edouard; Kristensson, Elias; Hottenbach, P.; Aldén, Marcus; Gruenefeld, G.

Published in:
Applied Physics B

DOI:
10.1007/s00340-012-5237-9

2012

Document Version:
Publisher's PDF, also known as Version of record

Three-dimensional measurement of the local extinction coefficient in a dense spray

Meas. Sci. Technol. **22** (2011) 125303 (15pp) doi:10.1088/0957-0233/22/12/125303

Three-dimensional measurement of the local extinction coefficient in a dense spray

Rikard Wellander, Edouard Berrocal, Elias Kristensson, Mattias Richter and Marcus Aldén

Division of Combustion Physics, Lund Institute of Technology, Box 118, Lund 221 00, Sweden

E-mail: rikard.wellander@forbrf.lth.se

Received 30 May 2011, in final form 15 September 2011
Published 31 October 2011
Online at stacks.iop.org/MST/22/125303

Abstract
Laser extinction, signal attenuation and multiple scattering are the three main phenomena limiting qualitative and quantitative measurements in planar laser imaging of sprays. In this paper, a method is presented where structured laser illumination planar imaging is used to remove the signal contribution from multiply scattered light. Based on this technique, data from side scattering and transmission measurements are obtained simultaneously. An algorithm, compensating for signal attenuation and laser extinction, is further applied to calculate the local extinction coefficient. The method is first demonstrated on a cuvette containing a homogeneous solution of scattering particles with an extinction coefficient $\overline{\mu}_e = 0.13\ \text{mm}^{-1}$. Finally the procedure is applied on an air-assisted water spray with a maximum optical depth of OD ~ 3, where the position-dependent extinction coefficient is extracted within the probed volume. To the best of our knowledge, this paper demonstrates for the first time a method to measure the local $\overline{\mu}_e$ within the three dimensions of an inhomogeneous scattering medium using laser sheet illumination, after suppression of the multiple light scattering intensity.

Keywords: multiple scattering, laser extinction, signal attenuation, extinction, coefficient, dense sprays, Mie scattering, structured illumination

(Some figures in this article are in colour only in the electronic version)

Nomenclature

M	recorded light scattered from the modulated laser sheet
S	calculated structured laser illumination planar imaging data
C	calculated conventional planar imaging data
S_{tr}	SLIPI data proportional to the irradiance of the transmitted laser sheet (induced fluorescence from a dye cell)
S_i	SLIPI data proportional to the initial energy in the laser pulse (induced fluorescence from a dye cell)
S_{sm}	SLIPI data from the scattering medium
I_i	irradiance of the initial/incident laser light
I_s	irradiance of the scattered light
I_f	irradiance of the transmitted/final laser light
K_a	constant relating S_{sm} to I_s, called camera function
K_b	constant relating S_i and S_{tr} to I_i and I_f (similar to K_a but also considering the concentration and quantum yield of the dye)
$\overline{\mu}_e$	averaged extinction coefficients in the scattering medium
a	attenuation between the scattering event and the camera

1. Introduction

Sprays are two-phase flow systems defined by a heterogeneous and polydisperse collection of individual droplets. They are employed for numerous applications ranging from fuel injection in combustion engines to medical spray treatments. The ability to measure spray characteristics is of fundamental importance both for the further understanding of break-up mechanisms as well as for the optimization and control of spray-assisted systems. Measurements of local droplet size and concentration have been performed, in the past, by a

variety of well-established laser-based techniques, such as phase Doppler interferometry [1, 2], low angle light scattering [3], planar droplet sizing [4, 5] and interferometric laser imaging droplet sizing [6, 7]. These techniques assume that only one scattering event has occurred for each detected photon. Such an assumption is valid in the single scattering regime (where the average number of scattering events is less than 1) corresponding to a light transmission of $I_f/I_i \geqslant 0.37$. The light transmission can be described by the Beer–Lambert law as

$$I_f/I_i = e^{-OD} = e^{-\overline{\mu}_e \cdot l}, \tag{1}$$

where I_i and I_f represent the initial and final/transmitted irradiance, OD is the optical depth and l is the distance the laser beam has propagated through a medium with average extinction coefficient $\overline{\mu}_e$. In the case of qualitative imaging of sprays, $\overline{\mu}_e$ is in fact the probed physical quantity. By definition, the averaged extinction coefficient is expressed as

$$\begin{aligned}\overline{\mu}_e &= N \cdot (\overline{\sigma_s} + \overline{\sigma_a}) \\ &= N \cdot \frac{\int_0^\infty n_p(D) \cdot (\sigma_s(D) + \sigma_a(D)) \cdot dD}{\int_0^\infty n_p(D) \cdot dD},\end{aligned} \tag{2}$$

where N is the number density of droplets, $n_p(D)$ is the number of droplets with diameter D and σ_s and σ_a are the scattering and absorption cross sections, respectively. Thus, the extinction coefficient is an important property of sprays containing information related to both particle size and number density. With the extinction coefficient known, a complementary measurement (using, for instance, laser-induced fluorescence (LIF) [4, 5], Raman scattering [8, 9], polarization ratio [10], or elastic scattering at a different wavelength [11]) of either size or number density would directly yield the other quantity.

Laser sheet illumination is an attractive technique for two-dimensional mapping of volumetric two-phase flows thanks to its small depth of field and large field of view. However, when imaging an optically dense medium, several artifacts are introduced in the measurement, strongly limiting both quantitative and qualitative treatment of the data.

First, the light propagating through a turbid medium interacts with the particles through scattering and absorption. The irradiance of the unperturbed light thereby decreases exponentially as a function of the distance. This phenomenon is commonly referred to as laser extinction and is described by equation (1). Several methods have been developed to compensate or correct for laser extinction. Hertz *et al* [12] measured the fluorescence and the attenuation of the exciting laser light in an absorbing flame. An iterative computer algorithm was, in this case, used to compensate for the laser extinction in order to extract the OH concentration. Versluis *et al* [13] measured the number density of fluorescing OH from two images where the illuminating laser sheets were propagating in opposite directions. The influence from laser extinction was circumvented by taking the derivative of the logarithm of the ratio between the two images. The main drawback with such an approach is the low signal-to-noise ratio. Note that Talley *et al* [14] applied a similar approach with counter-propagating laser sheets through a fluorescing hollow-cone spray and a flat fan spray. Abu-Gharbieh *et al* [15] recorded the Mie-scattered light from an optically dense spray. Laser extinction was in this case compensated for by assuming the spray to be symmetric around its centerline.

Laser extinction is not the only source of error when imaging a scattering medium (SM). The scattered light that is to be detected also suffers from attenuation along its path to the detector. This second loss of light is, as for laser extinction, described by equation (1). Sick *et al* [16] presented a simple way to give a rough estimate of the fluorescence signal attenuation by placing an illuminated dye cuvette (DC) behind the spray. Koh *et al* [17, 18] used two cameras to suppress unwanted errors introduced by signal attenuation. Instead of trying to measure it, Kalt *et al* [19] suggested to use a large camera objective aperture in order to homogenize the effect of the signal attenuation on the final images. However, increasing the numerical aperture also increases the amount of multiply scattered light detected [20], a source of error which is not corrected for in the methods described above.

By definition, multiple scattering is the event of a photon being scattered by more than one individual particle. Any photon that has been scattered more than once loses information regarding where the first scattering event took place and is falsely interpreted as originating from a different location. In dense sprays, the effects of multiple scattering are particularly severe [20, 21], making correction algorithms for laser extinction and signal attenuation unreliable. One technique reducing the contribution of multiple scattering intensity is to scan the sample with a narrow Gaussian laser beam rather than a laser sheet and to use a small detection acceptance angle [20, 22–24]. It may also be partly suppressed by means of polarization filtering [11]. However, for an extensive reduction of the signal generated by multiple scattering and detected in laser sheet imaging, a technique called structured laser illumination planar imaging (SLIPI) has recently been developed and is described in [25–28]. The method is based on applying a sinusoidal intensity pattern along the height of a laser sheet. If the modulation is fine enough, the origin of multiply scattered light becomes independent of the modulation pattern, whereas the position of the first scattering events remains dependent on it. Thus, the amplitude of the modulated component acts as a signature of the singly scattered light. While shifting the phase in the spatial period of the modulation $(n-1)$ times in steps of $2\pi/n$ ($n \geqslant 3$), a series of n modulated images, M_i, are recorded, where i denotes the phase of the modulation. From these images, the modulated part, representing mainly the singly scattered light, can be extracted to form the SLIPI data S according to

$$S = \frac{\sqrt{2}}{n}\left(\sum_{i=1}^{n-1}\sum_{j=i+1}^{n}(M_i - M_j)^2\right)^{1/2}. \tag{3}$$

Recently, SLIPI has been used with a dual camera setup (dual-SLIPI) to enable the calculation of the extinction coefficient in a plane with limited depth resolution [29]. Here, SLIPI is used for three-dimensional measurements, where

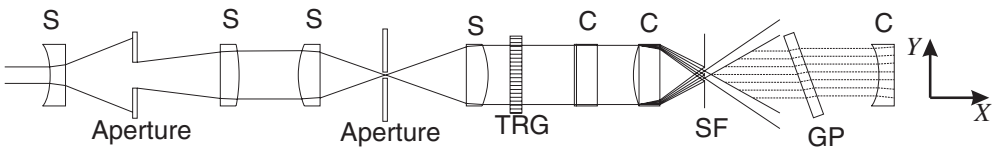

Figure 1. Schematic drawing of the optical arrangement as seen from the side. S: spherical lens, C: cylindrical lens, TRG: transmission Ronchi grating, SF: spatial filter, GP: glass plate. The light propagates in the positive *X*-direction.

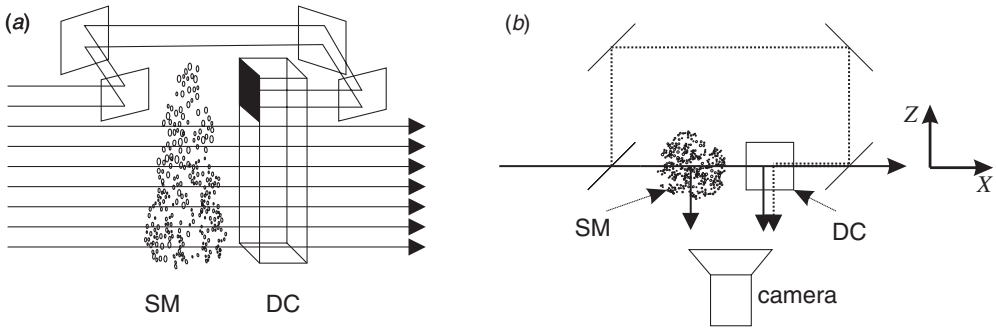

Figure 2. Schematic drawing of the experimental setup with the SM to be investigated and the DC, containing a solution of Rhodamine 6G in methanol, used for the transmission measurements. A portion of the laser sheet is redirected to illuminate the upper part of the DC from the opposite direction. This enables laser intensity fluctuations to be recorded over time. Note that the field of view of the camera includes both SM and DC. (*a*) Perspective view, (*b*) top view of the setup.

scattered light from the probed medium as well as the incident and transmitted irradiance of the illuminating laser sheet is simultaneously recorded. These data are processed using an algorithm developed in-house which calculates the local extinction coefficient throughout the probed volume. In this paper, the experimental setup and procedure are first described. Then the successive steps of the algorithm are detailed. To validate both the reliability of the experimental procedure and of the data post-processing, the method is tested on a homogeneous sample of polystyrene microspheres immersed in distilled water. Finally, the approach is applied to an air-assisted water spray with a maximum optical depth of OD = 3, corresponding to ∼5% light transmission.

2. Description of the experiment

2.1. Experimental setup

The SM is illuminated by a pulsed Nd:YAG laser, emitting 532 nm radiation at 10 Hz. The optical arrangement to construct the modulated laser sheet for the SLIPI measurements is shown in figure 1. An aperture is used to select a near top hat profile of the laser beam that is spatially filtered for improved uniformity. A transmission Ronchi grating with a frequency of 5 lp mm^{-1} together with a series of cylindrical lenses is used to create a sinusoidal modulation along the height of the laser sheet. A 1 mm thick glass plate attached to a motorized rotational stage automatically shifts the modulation along the vertical direction.

The spatial period of the laser sheet intensity modulation within the SM is 1.15 mm.

Figure 2 illustrates the experimental setup. The SM under investigation is positioned by a micrometer translator which enables imaging at various depths. A 14 bit electron-multiplier CCD camera (Andor iXon-DV887, 512 × 512 pixels) is used to image both the SM and a dye cell containing a solution of Rhodamine 6G in methanol, within the same frame. A collection angle of 1.35° is obtained with a Nikkon 200 mm objective at $f/8$. The fluorescence from the dye cell is recorded to evaluate the irradiance of the transmitted light. In addition, a part of the laser sheet (approximately three periods of the modulation) is rerouted around the SM to illuminate the top of the dye cell from the opposite direction (see figure 2). This configuration enables the recording of the incident laser power.

2.2. Experimental procedure

The experimental procedure to extract the data required to calculate $\overline{\mu}_e$ in the three dimensions of a SM is shown in figure 3. For each step, the SLIPI data are extracted using equation (3). Note that only three modulated images are required when applying structured illumination. However, an increase in the number of modulated images decreases the appearance of residual lines in the final SLIPI image and increases statistics. Here, nine images were recorded for each SLIPI image ($n = 9$ in equation (3)). At first, the fluorescence from the DC is recorded without the SM. At this position, referred to as $m = 0$, the incident irradiance equals the transmitted irradiance. While the fluence of the laser sheet varies from shot to shot, its spatial profile is found to be constant over time. Hence, the data from the main part of the DC, averaged over its width, represent a fingerprint of the incident laser sheet profile at all other positions m although it is denoted as $S_{tr}(0)$. The averaged data from the upper part of the DC are proportional to the radiant energy of the incident laser sheet and are denoted as $S_i(0)$. $S_i(0)$ is later used to compensate for the fluctuations and drift in the laser sheet

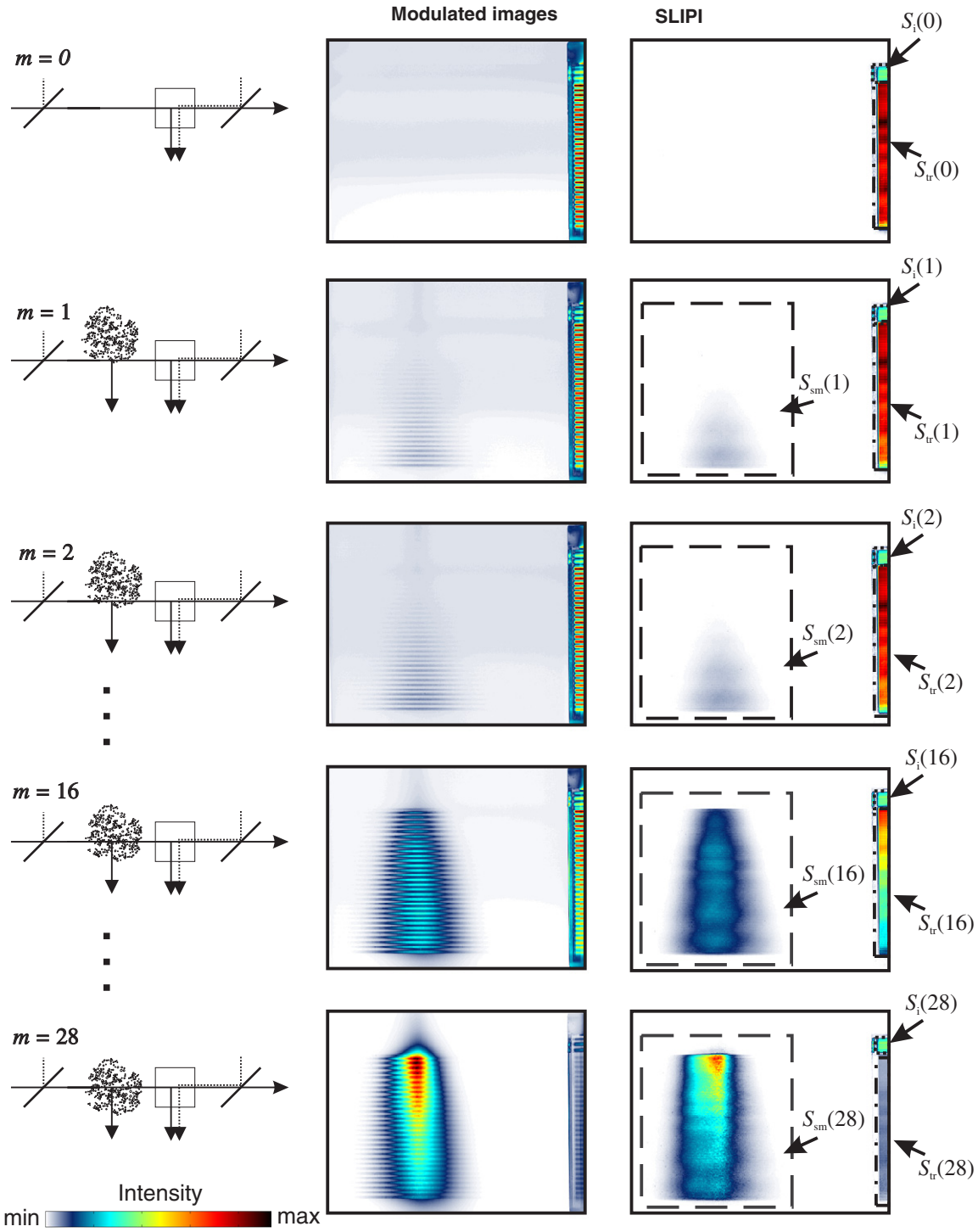

Figure 3. Schematic drawing of the scanning procedure. At each position m, a SLIPI image is constructed from nine modulated images using equation (3). At position $m = 0$, the data are recorded without any SM. At $m = 1$, the signal attenuation is assumed to be negligible. The successive layers are recorded with a separation of 500 μm. $S_i(m)$, $S_{tr}(m)$ and $S_{sm}(m)$ represent the SLIPI data from the upper part of the DC (averaged in 2D), from the main part of the DC (averaged over its width) and from the probed SM, respectively.

radiant energy. The second step is to extract SLIPI data with the SM present. At the first position, $m = 1$, the laser sheet illuminates the outermost part of the SM, from where the signal attenuation is assumed to be negligible. Thereafter the sample is moved with equidistant steps of 500 μm perpendicular to the laser sheet, and the data required to form one SLIPI image are recorded at each successive position $m = 1, 2, 3 \ldots$ (see figure 3). At these positions, the transmitted laser sheet has been affected by laser extinction due to the scattering particles in its path. Thus, unlike $S_{tr}(0)$ which is a measure

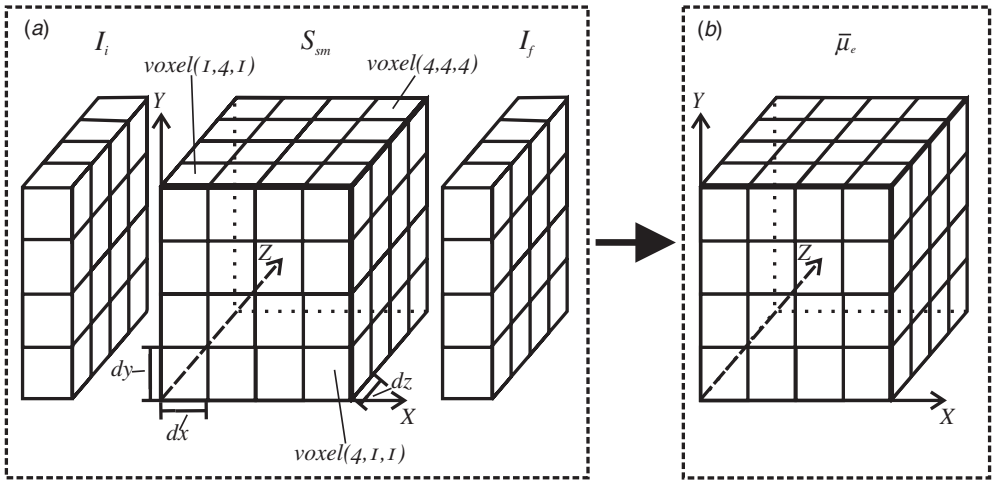

Figure 4. (*a*) Matrix representation of the experimental data required for the calculations of $\overline{\mu}_e$. One 2D matrix contains the incident irradiance of the laser sheet I_i, one 2D matrix contains the final irradiance I_f and one 3D matrix contains the data from the SM S_{sm}. (*b*) After postprocessing the input data given in (*a*), using the algorithm presented in section 3, a 3D matrix of the extinction coefficient $\overline{\mu}_e$ is obtained.

of the incident irradiance, $S_{tr}(m > 0)$ is proportional to the transmitted/final light irradiance according to

$$I_f(m) = K_b \cdot S_{tr}(m), \tag{4}$$

where K_b is a constant containing the collection efficiency of the detection system and the concentration and quantum yield of the dye. The incident irradiance, when the SM is at position $m > 0$, is obtained from $S_{tr}(0)$ and the measurement of the relative change in radiant energy of the incident laser sheet from plane zero to plane m:

$$I_i(m) = K_b \cdot S_{tr}(0)\frac{S_i(m)}{S_i(0)}. \tag{5}$$

The 'singly' scattered light intensity from the SM is obtained from the SLIPI image and is denoted by $S_{sm}(m)$ in figure 3.

At the end of the experimental procedure, the collected data are as follows:

- I_i/K_b, 2D matrix proportional to the incident irradiance.
- I_f/K_b, 2D matrix proportional to the transmitted irradiance.
- S_{sm}, 3D matrix with voxels, containing the data from the volume spanned by the area of a pixel in the imaging plane ($dx \cdot dy$) and the distance between two adjacent laser sheets (dz). The voxels are indexed voxel (k, l, m) where k, l and m represent the number of voxels along X, Y and Z, respectively.

Note that even though S_{sm} is corrected from effects introduced by multiple scattering using SLIPI, the data still suffer from laser extinction and signal attenuation. The three matrices, which are illustrated in figure 4(*a*), serve as input data for the calculation of the extinction coefficients (figure 4(*b*)).

3. Method to calculate the extinction coefficient

3.1. General description of the algorithm

The algorithm developed in this paper extracts the extinction coefficients from the experimental data in a similar 'bread slicing' manner as presented in [22, 23]. To account for the light intensity reduction due to signal attenuation, at each given position $m = i$ of the laser sheet, the algorithm uses the extinction coefficient previously calculated at all positions $m < i$ (between the illuminated plane and the camera). This procedure implies that the attenuation of the signal generated at the first position $m = 1$ must be known in advance. Such a condition can be arranged experimentally by illuminating the edge of the SM where signal attenuation is assumed negligible.

For a general understanding, the algorithm is first described in a simplified step by the step procedure, followed in the next subsection by a more detailed derivation. As depicted in figure 5, the algorithm can be divided into the following steps:

- in step 1, data corresponding to the incident irradiance, I_i, the final irradiance, I_f, and the light scattered from within each voxel, S_{sm}, are extracted from the SLIPI image at position $m = i$, i.e. the XY-layer at one of the positions on the Z-axis in figure 4;
- in step 2, the total loss in irradiance due to laser extinction is calculated by subtracting the transmitted irradiance from the incident irradiance;
- in step 3, the local loss in irradiance within each imaged voxel is calculated from the total loss of irradiance (from step 2), the signal from the SM S_{sm} and the previously calculated extinction coefficients at positions $m < i$;
- in step 4, the irradiance before and after each voxel is deduced from the data calculated in step 3;
- in step 5, the extinction coefficient in each voxel, at $m = i$, is calculated based on the Beer–Lambert law using intensity values provided in step 4;
- in step 6, the extinction coefficients are added to the 3D matrix of previously calculated $\overline{\mu}_e$ (figure 4(*b*)) and the calculations are repeated for the position $m = i + 1$.

3.2. Theoretical derivation

The general procedure visualized in figure 5 can be theoretically derived by first expressing the SLIPI data

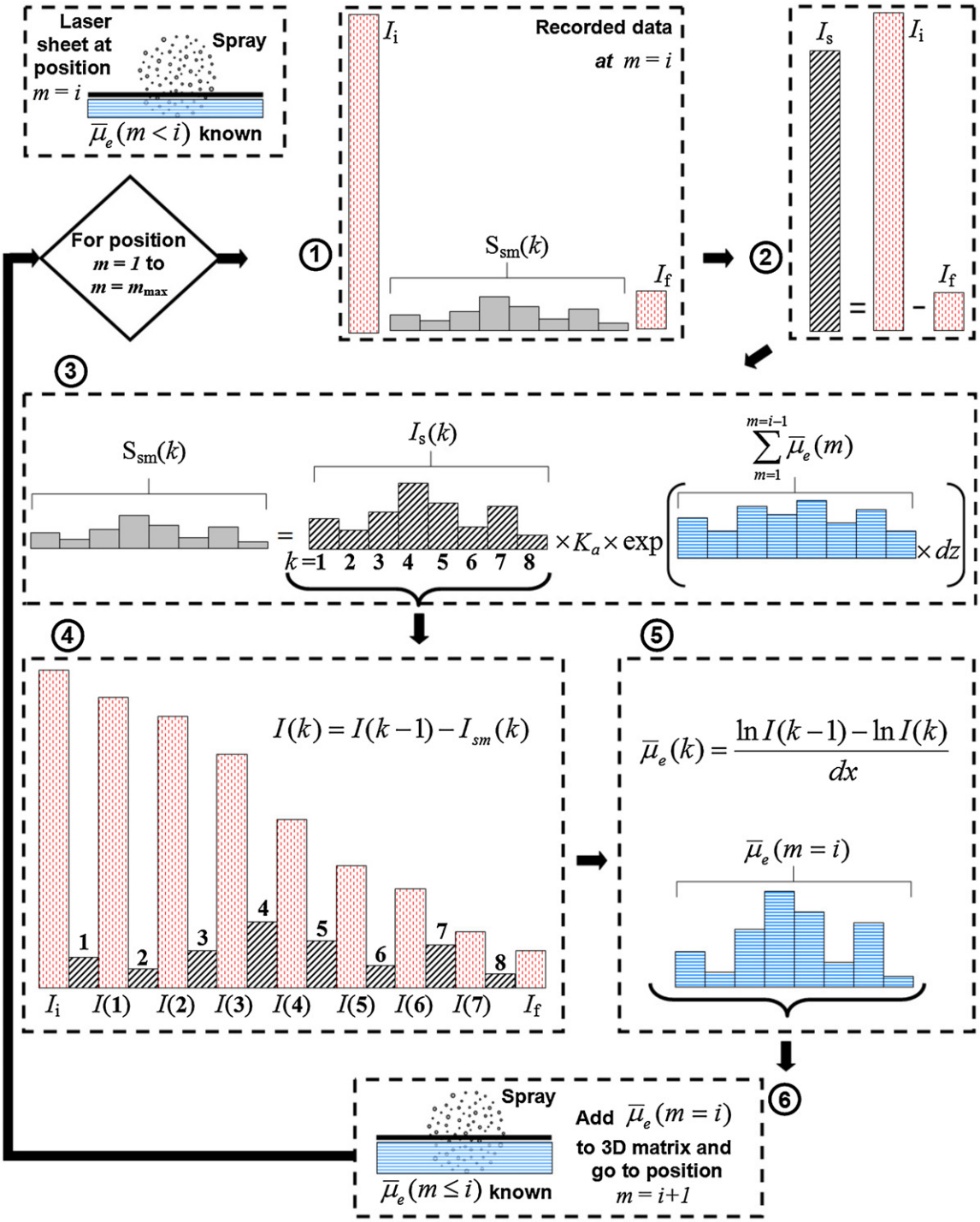

Figure 5. Description of the algorithm used to calculate $\overline{\mu}_e$ from the SLIPI data illustrated in figure 4(*a*). These input data are initially collected from the experimental procedure described in section 2.2. When the algorithm calculates $\overline{\mu}_e$ at position $m = i$, it uses the previously calculated $\overline{\mu}_e$ at positions $m < i$.

$S_{sm}(k, l, m)$, at pixels k and l and image m (corresponding to voxel (k, l, m) in the SM) as

$$S_{sm}(k, l, m) = I_s(k, l, m) K_a(k, l, m) (1 - a(k, l, m)), \quad (6)$$

where $I_s(k, l, m)$ represents the irradiance scattered within voxel (k, l, m), $K_a(k, l, m)$ is the camera function (solid angle of collection times camera efficiency) and $a(k, l, m)$ represents the signal attenuation as the light propagates from voxel (k, l, m) through the SM to the camera. Note that the term $(1-a(k, l, m))$ represents the light transmission. By assuming a 0° acceptance angle and negligible attenuation outside the probed volume, the signal attenuation equals

$$a(k, l, m) = 1 - \exp\left(-\sum_{m'=0}^{m-1} \overline{\mu}_e(k, l, m')\, dz\right), \quad (7)$$

where $\overline{\mu}_e(k, l, m')$ is the average extinction coefficient in voxel (k, l, m'). An expression of the scattered irradiance $I_s(k, l, m)$ is obtained by rearranging equation (6):

$$I_s(k, l, m) = \frac{S_{sm}(k, l, m)}{K_a(k, l, m)\,(1 - a(k, l, m))}. \quad (8)$$

The unknown camera function, $K_a(k, l, m)$, in equation (8) could be estimated from the solid angle of collection, property of the lenses and quantum efficiency and fill factor of the camera. However, this is difficult and likely introduces errors. Here it is instead estimated by utilizing the fact that the sum of the scattered light from each voxel along a row of voxels in the direction of the laser sheet propagation is equal to the difference between the incident and transmitted/final irradiance of the laser light (step 2 in figure 5):

$$\sum_{k=1}^{k_{max}} I_s(k, l, m) = I_i(l, m) - I_f(l, m), \quad (9)$$

where $I_i(l, m)$ is the incident irradiance (at voxel $(0, l, m)$) and $I_f(l, m)$ is the transmitted irradiance (at voxel $(k_{max}+1, l, m)$). Combining equation (8) with (9) yields

$$\sum_{k=1}^{k_{max}} \frac{S_{sm}(k, l, m)}{K_a(k, l, m)\,(1 - a(k, l, m))} = I_i(l, m) - I_f(l, m). \quad (10)$$

Since the distance between the SM and camera is much larger than the width of the imaging area, the camera function $K_a(k, l, m)$ is assumed to be independent of k and can thus be moved outside the summation in equation (10). $K_a(k, l, m)$ can then be expressed as

$$K_a(k, l, m) = \frac{\sum_{k=1}^{k_{max}} \frac{S_{sm}(k, l, m)}{(1 - a(k, l, m))}}{I_i(l, m) - I_f(l, m)}, \quad (11)$$

i.e. the sum of the signal over the laser path (corrected for signal attenuation) divided with the loss of irradiance over the same path. To obtain an expression of the scattered irradiance, K_a in equation (8) is replaced with the expression in (11) (step 3 in figure 5)

$$I_s(k, l, m) = \frac{S_{sm}(k, l, m)(I_i(l, m) - I_f(l, m))}{(1 - a(k, l, m)) \sum_{k=1}^{k_{max}} \frac{S_{sm}(k, l, m)}{(1 - a(k, l, m))}}. \quad (12)$$

The only unknown parameter in equation (12), except for the constant K_b hidden in $I_f(l, m)$ and $I_i(l, m)$ (see equations (4) and (5)), is the signal attenuation. However, since the plane closest to the camera is located at the edge of the SM, the attenuation of the signal generated within this plane can be neglected ($a(k, l, 1) = 0$). Hence, for $m = 1$ the relative scattered irradiance $I_s(k, l, 1)/K_b$ can be calculated from the recorded data using equation (12).

The next step (step 4 in figure 5) in order to calculate the extinction coefficients is to calculate the position-dependent laser irradiance in between the voxels where the scattered irradiance has been calculated. This is done by subtracting the irradiance scattered within a voxel from the irradiance of the laser sheet before it enters that voxel:

$$I(k + 1, l, m) = I(k, l, m) - I_s(k, l, m). \quad (13)$$

Since the relative irradiance of the incident laser sheet is known from equation (5), the relative irradiance $I(k, l, m)/K_b$ can be calculated, one column at the time, in the direction of the laser sheet in layer $m = 1$ where $I_s(k, l, 1)/K_b$ is known.

The irradiance before and after each voxel can also be expressed with the attenuation of the light according to the Beer–Lambert law,

$$I(k + 1, l, m) = I(k, l, m) \exp(-\overline{\mu}_e(k, l, m)\,\mathrm{d}x). \quad (14)$$

Hence, the expression of the extinction coefficient is obtained by inserting equation (13) into (14) and rearranging (step 5 in figure 5),

$$\overline{\mu}_e(k, l, m) = -\ln\left(\frac{I(k, l, m) - I_s(k, l, m)}{I(k, l, m)}\right)\frac{1}{\mathrm{d}x}. \quad (15)$$

Equation (15) is fully determined since the unknown constant K_b in $I(k, l, m)$ and $I_s(k, l, m)$ cancels out in the division. With this equation the absolute extinction coefficient in the plane $m = 1$ is calculated. In the $m = 2$ plane, the signal attenuation is calculated from equation (7) whereafter equation (12) is used to calculate the relative scattered irradiance. The relative local irradiance is then calculated with equation (13) which enables the calculation of the position-dependent extinction coefficients (equation (15)). The procedure is repeated, for each position m, until $\overline{\mu}_e$ has been calculated for each voxel in the entire 3D matrix.

4. Validation of the method in a homogeneous SM

4.1. Comparison between SLIPI and conventional planar imaging

To validate the presented method, an experiment is conducted on a homogeneous SM. In this case, the same extinction coefficient should be measured in all locations of the probed volume. The medium of interest consists of a glass cuvette containing a homogeneous mixture of 0.5 μm monodisperse and non-absorbing polystyrene microspheres immersed in distilled water. Following the procedure described in section 2.2, 16 SLIPI images, separated by a distance of $\mathrm{d}z = 500$ μm, are extracted. In this analysis, a comparison is made between the method with multiple scattering suppression, using SLIPI, and without the suppression, assuming conventional laser sheet imaging. The conventional planar image can be constructed by averaging the n modulated images M according to

$$C = \frac{1}{n}\sum_{i=1}^{n} M_i. \quad (16)$$

A top view of the conventional data, constructed from nine modulated images M according to equation (16), is shown in figure 6(*a*), whereas the corresponding SLIPI data, constructed according to equation (3), are plotted in figure 6(*b*). In both figures, the intensity values are averaged along the vertical direction (Y-axis) of the cuvette. To independently examine the effects of laser extinction and signal attenuation, the logarithm values of the light intensity at $z = 0$ (no signal attenuation) and at $x = 0$ (no laser extinction) have been extracted and plotted in figures 6(*c*) and (*d*), respectively.

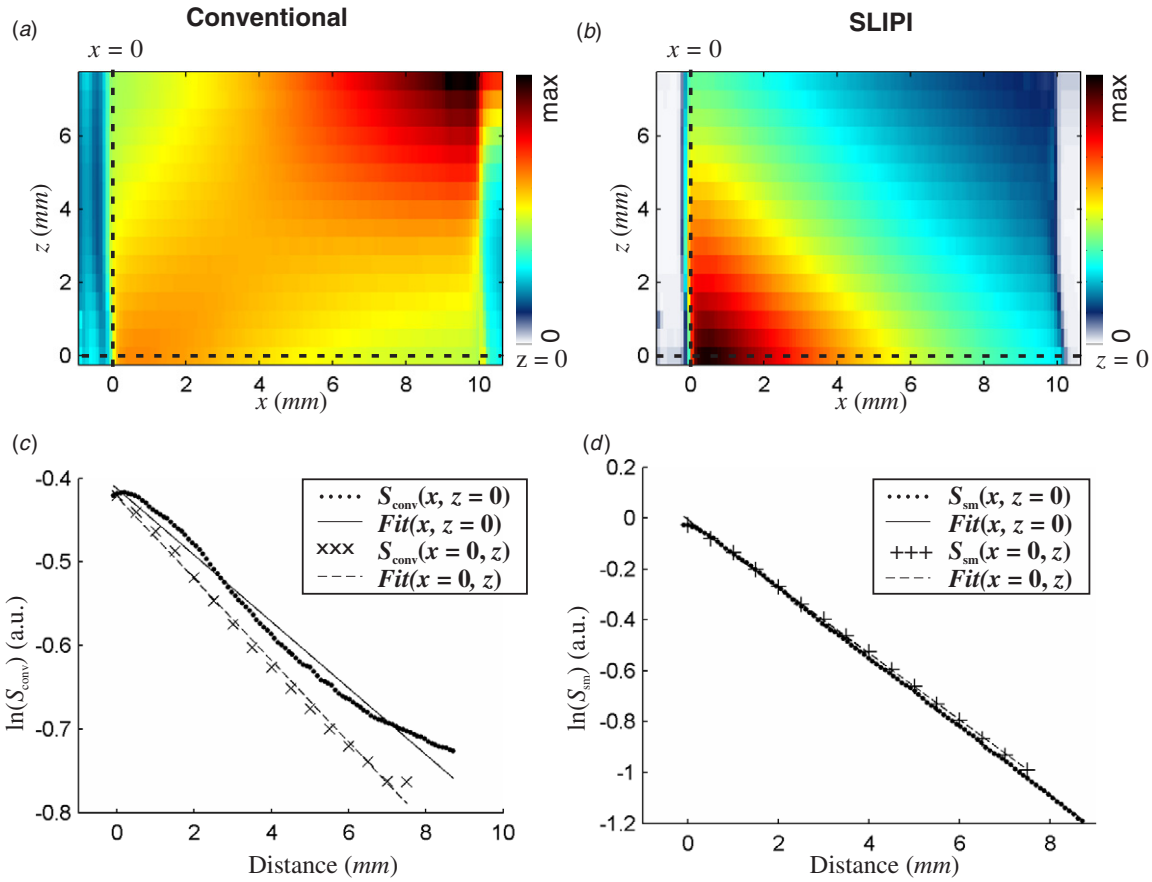

Figure 6. (*a*), (*b*) Top view of conventional and SLIPI data, respectively. The values are averaged along the height of the cuvette and normalized to its maximum value. The figures are constructed from 16 layers separated by 500 μm. (*c*), (*d*) A natural logarithm of the respective conventional and SLIPI data along the dashed lines indicated in (*a*) and (*b*). The best exponential fit of each curves is also indicated. Note that for the SLIPI case, in (*d*), all curves overlap by following the same exponential decay.

It is observed in figures 6(*b*) and (*d*) that the SLIPI data decrease exponentially, both along the *X*-direction, when $z = 0$, and along the *Z*-direction, when $x = 0$. However, such behavior is not observed in the conventional data which instead show complex spatial intensity fluctuations as seen in figures 6(*a*) and (*c*). In this case, the highest intensity value is obtained at position ($x = 10$ mm, $z = 8$ mm), which is most affected by laser extinction and signal attenuation, and should instead show the lowest intensity value. This counter-intuitive effect is attributed to the strong contribution of the multiple light scattering intensity. When suppressing this unwanted intensity, the extinction coefficient is directly represented by the slope of the plotted curves. Since the scattering is elastic and the medium homogeneous, the same extinction must be observed for the incident light along the *X*-axis as for the scattered light along the *Z*-axis. This is confirmed in the SLIPI results with the overlapping of the two curves given in figure 6(*d*), indicating that the intensity contribution from multiple scattering is successfully removed. Based on these results, the correct extinction coefficient can be extracted from the slope of the best exponential fit of the SLIPI curves along a single axis *X* or *Z*. It is found, from this approach, that $\overline{\mu}_e = 0.132\ \text{mm}^{-1}$.

4.2. Calculation of $\overline{\mu}_e$ from SLIPI and conventional planar imaging data

In the previous subsection, the extinction coefficient was estimated from the best exponential fit of the SLIPI data. In this subsection, the calculation of the extinction coefficient is performed in 3D, using the algorithm presented in section 3 and where the input data are either SLIPI or conventional images calculated with equations (3) and (16), respectively. A comparison between the results based on the conventional data, in (*a*), and the SLIPI data, in (*b*), is provided in figure 7. These images represent the top view of the cell which has been scanned with 16 successive positions of the laser sheet. The values of the extinction coefficient are averaged along the vertical direction (*Y*-axis) of the cuvette, resulting to a 2D view of $\overline{\mu}_e$ from the 3D calculated matrix. Also, the resultant extinction coefficients along $z = 0$ and $x = 0$, based on conventional data in figure 7(*c*), and SLIPI data in figure 7(*d*), are plotted to independently examine the effects of laser extinction and signal attenuation.

In figure 7(*a*), where the extinction coefficients are calculated without multiple scattering correction, variations of $\overline{\mu}_e$ ranging between $\sim$0.05 and $\sim$3.2 mm^{-1} can be observed. It is also seen that $\overline{\mu}_e$ is underestimated at the

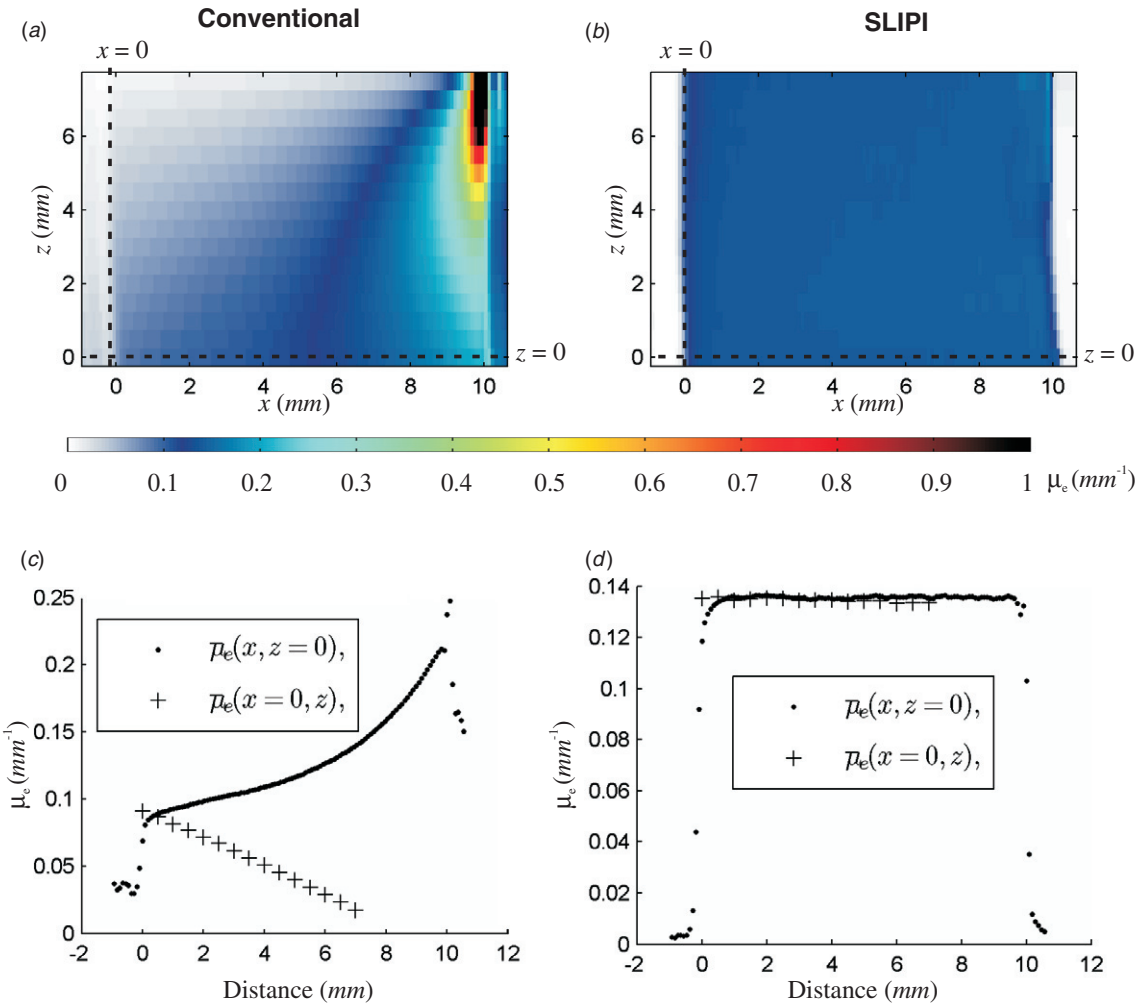

Figure 7. (*a*), (*b*) Top view of the extinction coefficient calculated from the conventional and SLIPI data, respectively. The values are averaged along the height of the cuvette. The figures are constructed from 16 layers separated by 500 μm. (*c*), (*d*) The extinction coefficient based on conventional and SLIPI data along the dashed lines indicated in (*a*) and (*b*).

entrance side of the laser sheet in the cell, at $x = 0$, and overestimated at the exit side, at $x = 10$ mm. Furthermore, the maximum extinction coefficient is calculated at position ($x = 10$ mm, $z = 8$ mm) which is most affected by intensity contributions from multiple light scattering (as mentioned in the subsection above). These effects are explained by the fact that the algorithm used here compensates for the exponential loss of light along the photon path, according to the Beer–Lambert law. The extra light introduced by multiple scattering is then interpreted as a higher scattering probability, resulting in a higher extinction coefficient given by the algorithm. As a result, the algorithm becomes inaccurate in the calculation of the extinction coefficient when the input data are contaminated by multiply scattered light (when the Beer–Lambert law is no longer valid). However, by extracting the single light scattering intensity using SLIPI, a quasi-homogeneous distribution of the extinction coefficient is found by the algorithm (shown in figures 7(*b*) and (*d*)), with an average value of $\overline{\mu}_e = 0.134$ mm^{-1} and a standard deviation of 0.017 mm^{-1}. This result is in agreement with the value of the extinction coefficient previously extrapolated from the curve fitting given in figure 6(*d*). Hence, these results validate both the suggested experimental procedure, using SLIPI, and the logic of the algorithm described in sections 2 and 3.

5. Application of the method to an air-assisted water spray

5.1. Initial results

The method validated above is applied on an air-assisted water spray generated by a Delavan AL-45 nozzle. The diameter of the orifice is 3 mm, producing a turbid spray with a cone angle of 15–20° in ambient air. With such an internal mixing nozzle, the atomization process is affected by both the air and the liquid injection pressures. In this investigation, pressures of 3 and 4.2 bar corresponding to the flow rates of 21 l h^{-1} and 175 l min^{-1} were used for the water and air, respectively. Due to the internal mixing, primary breakups occur already at the nozzle tip, producing a dense cloud of droplets with nominal diameter of $\sim$15 μm (size provided by the manufacturer). Following the experimental procedure described in section 2.2,

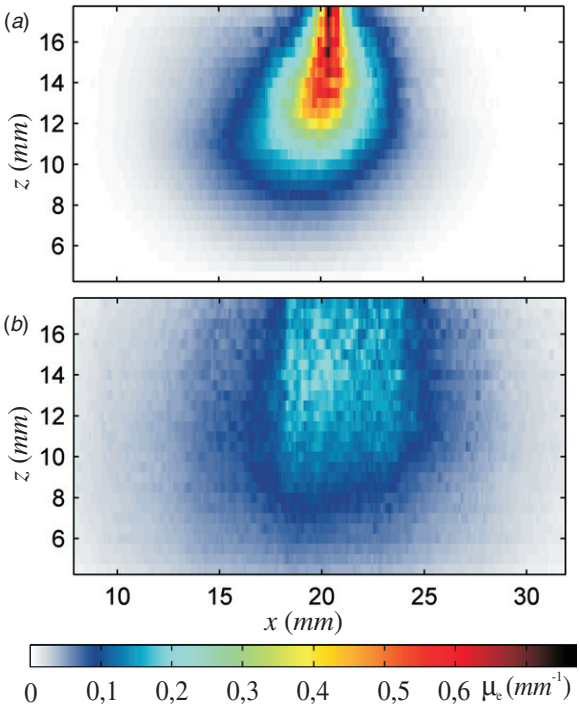

Figure 8. Horizontal sections of the extinction coefficient at 23 mm in (*a*) and 53 mm in (*b*) below the nozzle tip. These results correspond, respectively, to the top and bottom of the 3D extinction coefficient matrix illustrated in figure 4(*b*).

36 successive SLIPI images were recorded covering a spray volume of $40 \times 33.5 \times 17.5$ mm^3 in the X, Y and Z coordinate system. The top of the spray volume is located at 23 mm below the nozzle tip, beneath the region where the possible presence of a liquid core, ligaments and other large irregular liquid bodies could introduce errors in the calculation of the extinction coefficient, which requires independent scattering particles to be valid.

Figures 8(*a*) and (*b*) show two horizontal sections of the extinction coefficients at 23 and 53 mm below the nozzle tip, respectively. From these results, the global structure of the spray appears to be strongly asymmetric, especially in the densest region, at 23 mm below the nozzle orifice. Even though the spray is not perfectly symmetric, the severe asymmetry seen in figure 8 more likely originates from errors introduced in the measurement than from the intrinsic structure/geometry of the spray itself.

From the analysis given in the validation subsection 4.2, it was observed, for conventional planar imaging, that the algorithm tends to overestimate the extinction coefficient in regions affected by multiple scattering. The results in figure 8 reveal similar features, indicating that some intensity residuals from multiple light scattering still remain in the SLIPI images of the air-assisted spray. It has been shown in Monte Carlo simulations that although the SLIPI process effectively removes most of the multiply scattered light intensity, a part of it is, in some cases, not filtered out [30]. Two reasons can explain why this unwanted intensity remains in the SLIPI images of the spray and not in the SLIPI images of the SM used in the validation work. The first reason is the differences in particle size. Water droplets of $\sim$15 μm in air have 175 times higher probability to scatter light in the forward direction, between 0° and 1°, than $\sim$0.5 μm polystyrene spheres in water (calculated with the Mie theory at 532 nm illumination). The second reason is the the simple fact that the probed SM in the cuvette is not as optically dense as the spray. These two reasons make the filtering less efficient in the spray system than in the polystyrene dispersion investigated in this paper. Thus, an additional correction routine is required whenever the multiply scattered light intensity is not fully removed in the SLIPI process.

5.2. *Correction for multiple scattering intensity residuals*

In order to increase the accuracy in the measurement of the extinction coefficients, the residual information introduced by the multiply scattered light, in the SLIPI data, must be quantified and suppressed. Due to the strong capability of SLIPI in removing complex multiple scattering behavior, it can be assumed that the magnitude of these unwanted residuals is linearly related to the total number of scattering events and therefore also to the sum of the extinction coefficient along the photon path. With the knowledge of this relationship, the multiple scattering residuals could be removed from the initial SLIPI data.

One quantity that can provide a good indication about remaining multiple scattering intensity is the camera function K_a. As explained previously, K_a is related to the solid angle of the collection optics, the property of the detection lenses as well as the quantum efficiency and fill factor of the camera. Since neither the position nor the settings of the camera or collection optics are altered during the recordings (i.e. the same distance between the laser sheet and the camera and constant camera gain), K_a should remain constant at each position m of the laser sheet in the spray. According to equation (11), the camera function K_a is calculated from the relationship between the recorded scattered light S_{sm} and the extinction measurements $(I_i - I_f)$. Thus, an increased value of S_{sm} due to multiple scattering residuals also results in an increased value of K_a. By plotting K_a as a function of the sum of the extinction coefficient along the photon path, the variations of the camera function from a constant value can be visualized, providing indication about multiple scattering residuals contained in the SLIPI images.

In the derivation of the camera function, it is assumed to be constant as a function of x (see equation (11)). Therefore, the value of K_a for a specific voxel actually represents the averaged value of K_a for all voxels with the same position in Y and Z. Thus, the relationship between K_a and the sum of extinction coefficients along the photon path cannot be evaluated for each voxel individually. Instead the camera function is averaged over the full image for each position m to form $\langle K_a(m) \rangle$.

In figure 9, $\langle K_a(m) \rangle$ is plotted as a function of the sum of $\langle \overline{\mu}_e(m) \rangle$ between the laser sheet and the camera. In (*a*), the dispersion of polystyrene spheres shows a quasi-constant value of $\langle K_a(m) \rangle$. This expected observation validates the assumption of a constant camera function in the theoretical derivation. In this case, it is concluded that almost no

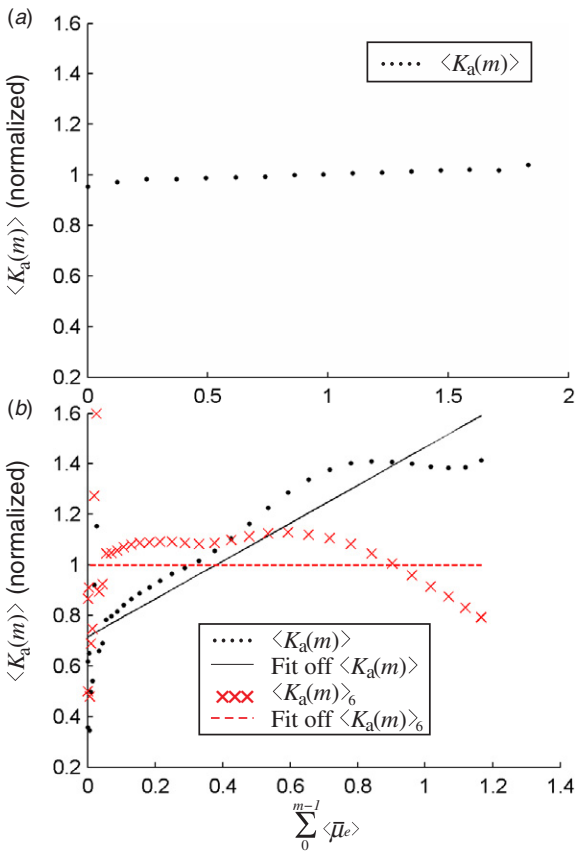

Figure 9. The averaged camera function $\langle K_a\rangle$ is plotted (black dots) for each image position m as a function of the sum of the average extinction coefficient at all positions $< m$. Note that an increase of the depth position ultimately leads to an increase in the sum of the extinction coefficient between the laser sheet position and the camera. (*a*) Cuvette measurements: $\langle K_a(m)\rangle$ remains quasi-constant demonstrating that the SLIPI images are not hampered by multiple scattering residuals. (*b*) Spray measurements: $\langle K_a(m)\rangle$ increases with the depth position of the laser sheet in the spray indicating the presence of multiple scattering residuals in the SLIPI data. A linear function is fitted to $\langle K_a(m)\rangle$ (solid line) and the original SLIPI data are iteratively corrected (six iterations), resulting in a new and more constant value of $\langle K_a(m)\rangle_6$, as shown by the crosses.

multiple scattering residual remains and no correction is needed.

On the other hand, for the spray medium shown in figure 9(*b*), $\langle K_a(m)\rangle$ increases with an increase of light attenuation between the laser sheet and the camera, corresponding to a deeper position m within the spray. As explained above, this increase is due to multiple scattering residuals in the initial SLIPI data, S_{sm}. To compensate for these residuals, S_{sm} is divided with the linear function obtained from a fit to the camera function (solid line in figure 9(*b*)),

$$S_{sm,2}(k,l,m) = \frac{S_{sm}(k,l,m)}{a + b\sum_{m'=0}^{m-1}\overline{\mu}_e(k,l,m')}. \qquad (17)$$

Here, a and b are the coefficients in the linear fit.

However, such a correction of the SLIPI data is solely based on the initially calculated extinction coefficients and camera function. If applied only once, this approach would not be accurate since these variables in turn are calculated from

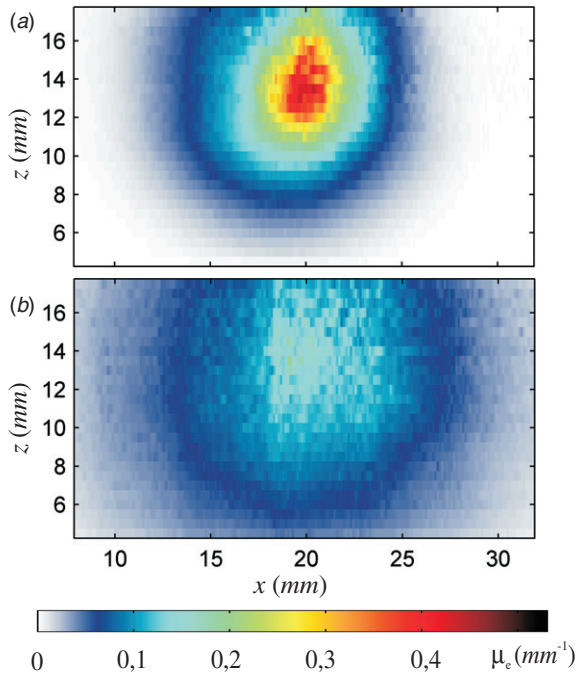

Figure 10. Resultant extinction coefficient after iteratively correcting the initial SLIPI data for multiple scattering residuals. This was performed by forcing the camera function $\langle K_a(m)\rangle$ to reach a constant value. These horizontal sections are located at 23 mm in (*a*) and 53 mm in (*b*) below the nozzle tip, corresponding, respectively, to the top and bottom of the 3D extinction coefficient matrix illustrated in figure 4(*b*). These results show a more symmetrical spray structure than without the intensity residuals' correction as shown in figure 8.

the initial SLIPI data S_{sm}. Also, the algorithm used to calculate the extinction coefficients estimates the attenuation from the extinction coefficients already calculated for the layers closer to the camera. Any trend in K_a as a function of Z (for instance, due to increasing multiple scattering) is therefore enhanced by the attenuation effect. Hence, the correction of the original SLIPI data must be iteratively refined by the corrected SLIPI data.

This is achieved by calculating the extinction coefficients from the compensated data, $S_{sm,2}$. This results in overcompensated extinction coefficients and a new camera function with an opposite but less pronounced trend than in the original camera function. By combining the linear fit of the original camera function with a linear fit of the new camera function

$$a = \sum_{n=1}^{N}(a_n) - (N-1), b = \sum_{n=1}^{N}\left(b_n \cdot \frac{a_1}{a_n}\right) \qquad (18)$$

and using the resulting coefficients for the calculations given in equation (17), a more accurate correction is obtained. By repeating this procedure in an iterative manner, $S_{sm,n}$ finally approaches a state where the slope of the new camera function b_n (dotted line in figure 9(*b*)) approaches zero. When this occurs, the correction also takes the signal attenuation into account.

The resulting extinction coefficients, plotted in figures 10(*a*) and (*b*), are more symmetrically distributed

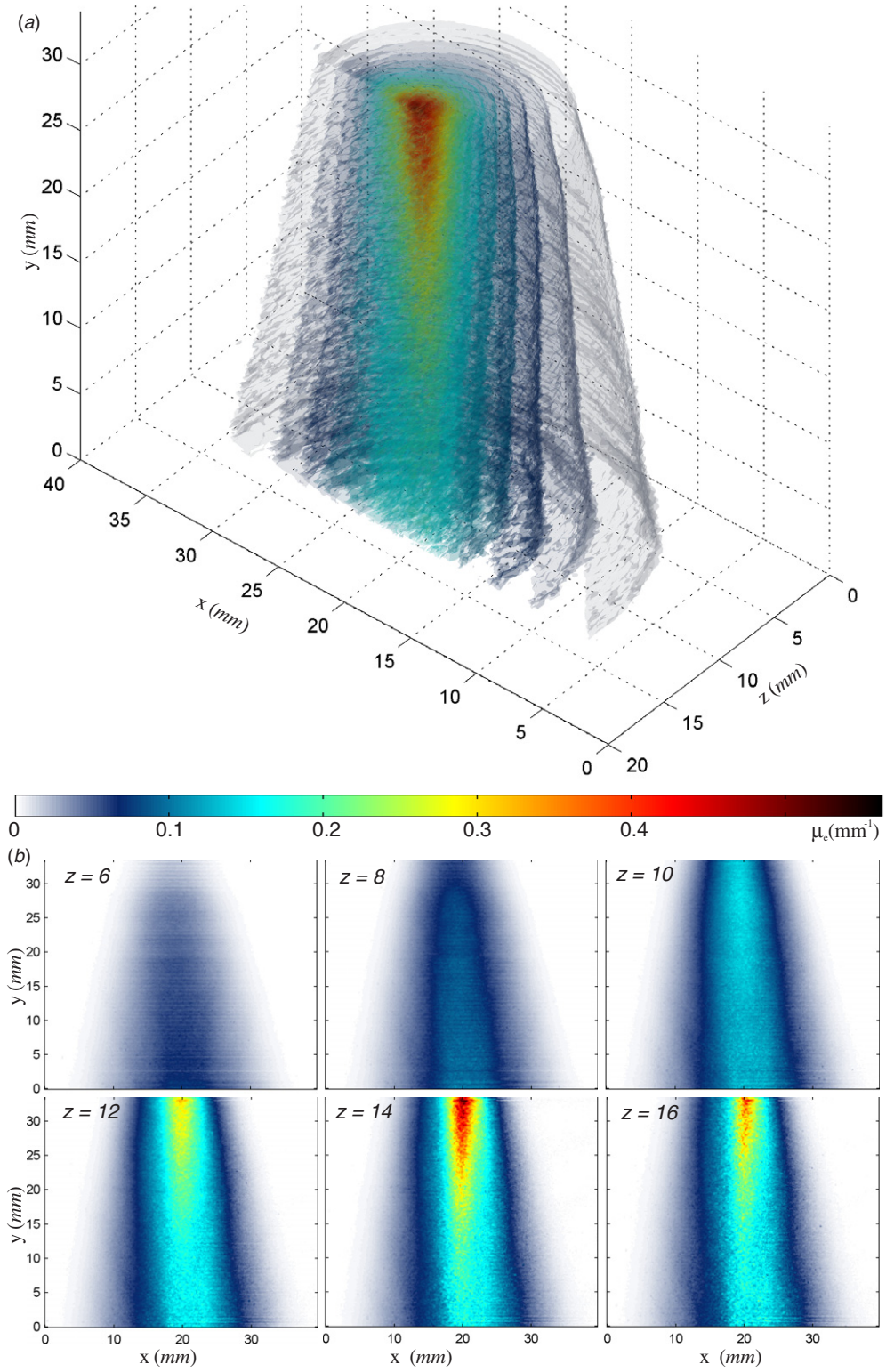

Figure 11. (*a*) 3D representation of the extinction coefficient covering a spray volume of 40 × 33.5 × 14 mm^3 in the *X*, *Y* and *Z* coordinate system (half of the spray). Note that the top of the spray volume is located at 23 mm below the nozzle tip. Isosurfaces are plotted for values between 3% and 98% of the maximum data value in steps of 5%. (*b*) Vertical sections of the extinction coefficient (as seen from the camera), at successive depth in the spray (distance indicated at the top-left corner of each image). The same scaling of the color bar is applied in (*a*) and (*b*).

than the corresponding extinction coefficients based on the uncorrected data (figures 8(*a*) and (*b*)) and are believed to more closely correspond to the true values of the extinction coefficients in the spray.

To calculate the accuracy of the measured extinction coefficients, the underlying errors need to be estimated. The major contribution to these errors originates from multiply scattered light that has not been fully filtered in the SLIPI

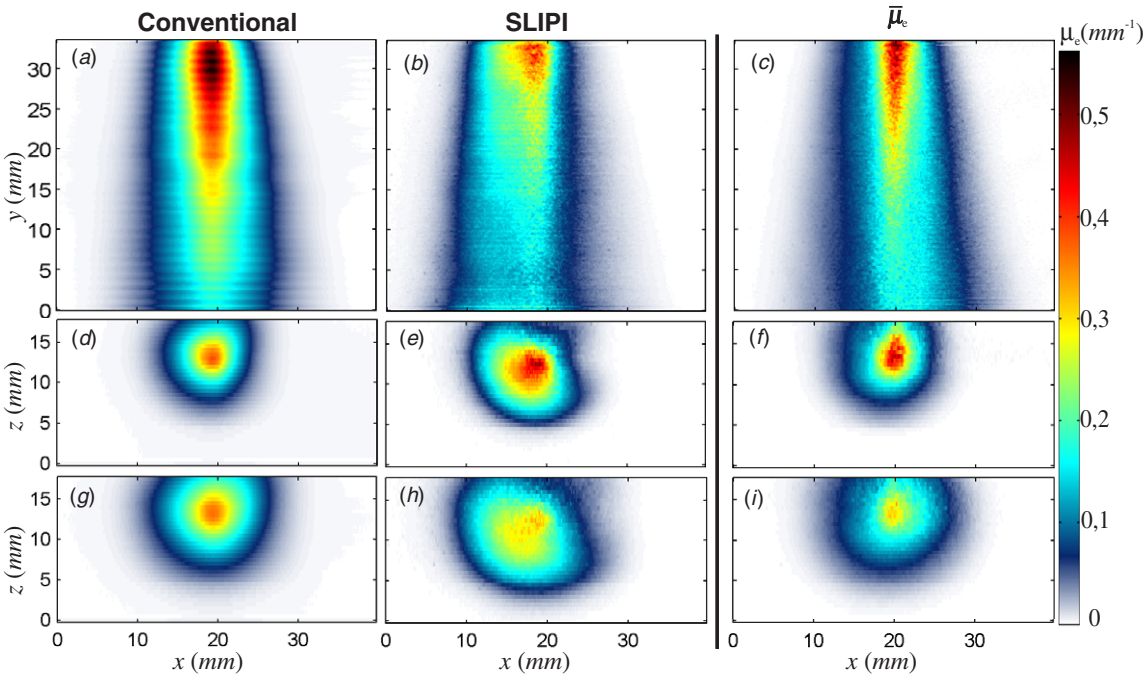

Figure 12. Images of the conventional, SLIPI and the extinction coefficient data. Parts (*a*)–(*c*) are plotted as seen from the camera (front view) at the center of the spray. Parts (*d*), (*e*) and (*g*), (*i*) are plotted as seen from above the spray (top view) at 23 and 35 mm from the nozzle, respectively. The data are scaled to the maximum value in each of the data matrices (conventional SLIPI or $\overline{\mu}_e$). In the conventional and SLIPI images, the units are arbitrary, while in the images of the extinction coefficients, the numbers shown in the color bar to the right have the units mm^{-1}.

process. To accurately estimate the magnitude and spatial distribution of the remaining residuals of multiple scattered light, Monte Carlo simulations could be used [20, 21, 30, 31]. However, this is beyond the scope of this paper.

5.3. Final results

Applying the correction for unwanted intensity residuals, described above, a realistic three-dimensional measurement of the local extinction coefficient is achieved. The probed volume is located at 23 mm below the nozzle tip, where light transmission reaches a minimum value of 5%. A three-dimensional representation of the data between $0 \leqslant z \leqslant 14$ mm, corresponding to one-half of the spray, is shown in figure 11(*a*). Isosurfaces are here plotted for values ranging from 3% to 98% of the maximum extinction coefficient in steps of 5%. To further investigate the variation in $\overline{\mu}_e$ throughout the spray, six vertical cross sections at successive positions along the *Z*-axis are shown in figure 11(*b*). At $z = 6$ mm, corresponding to the outer part of the spray, it is observed that the extinction coefficient is relatively homogeneous with a nominal value in the order of 0.05 mm^{-1}. In the center of the spray, at $z = 14$ mm, the extinction coefficient is instead highly inhomogeneous with a maximum value reaching 0.55 mm^{-1}. Note that if the spray were monodisperse, this would correspond to an increase in droplet concentration by a factor of 9, between the edge and the spray center. Another feature that can be noted is the spray symmetry around the central axis. By comparing the results between $z = 12$ mm and $z = 16$ mm, it is observed that this symmetry is well respected.

A comparison between conventional planar imaging, SLIPI and the measurement of the extinction coefficient is shown in figure 12. Figures 12(*a*)–(*c*) are vertical cross sections in the center of the spray corresponding to the depth position $z = 14$ mm, while figures 12(*d*)–(*f*) and 12(*g*)–(*i*) are horizontal cross sections at vertical distances $y = 23$ mm and $y = 35$ mm from the nozzle tip, respectively.

Even though the conventional planar images are strongly affected by multiple light scattering effects, it appears as if the spray is symmetric. By filtering out these unwanted intensities, the SLIPI images of the spray become particularly asymmetric, with an increase of signal suppression along the positive direction in *X* and *Y*. This asymmetry is a clear indication that effects from laser extinction and signal attenuation are severe in the spray. In the conventional images, such effects are hidden by the contribution from multiple scattering. Thus, the fact that the symmetry is conserved in the conventional data does not guarantee that the signal attenuation and laser extinction can be neglected. By calculating the extinction coefficients using the presented algorithm, the spray symmetry is restored but with a shape that is clearly different to the one based on the conventional data.

One should therefore be careful when drawing qualitative conclusions from conventional planar images based solely on the fact that signal attenuation and laser extinction are not visible. When using SLIPI, these effects are highlighted thanks to the multiple light scattering intensity suppression. Finally, the image of the extinction coefficient distribution provides a more reliable qualitative representation of the real spray structure.

6. Conclusion

A method has been developed to reveal the position-dependent extinction coefficient within the three dimensions of an inhomogeneous SM. This has been achieved by combining the ability of SLIPI to suppress the multiply scattered light intensity with both an experimental procedure and a post-processing algorithm.

The method has been validated on a homogeneous SM of monodisperse polystyrene spheres dispersed in distilled water. As expected, a homogenous extinction coefficient was measured within the entire probed volume, corresponding to $\overline{\mu}_e = 0.13\ \text{mm}^{-1}$. A comparison of the results with conventional planar imaging clearly demonstrates that the three-dimensional measurement of $\overline{\mu}_e$ was not applicable when the intensity from multiple light scattering was not suppressed beforehand, even for the relatively low extinction coefficients used in the experiment.

The method has further been applied to a dense air-assisted water spray. In this case, it was found that although most of the multiple light scattering intensity was removed, some unwanted residuals remained in the SLIPI images resulting in a non-symmetrical structure of the spray. An iterative correction routine has been developed to suppress the remaining multiple scattering intensity residuals in the SLIPI images. From the presented results, it has been observed that the measured extinction coefficient does not only reveal quantitative information of the spray properties, but also shows that qualitative conclusions drawn from conventional planar laser sheet imaging can be highly ambiguous.

The ability to measure the extinction coefficient, as described in this paper, enables future measurements where dense sprays could be fully characterized in three dimensions in terms of droplet number density and size distribution.

Acknowledgments

The authors wish to thank the Linné Center within the Lund Laser Center (LLC) as well as the CECOST through SSF and STEM for financial support. Also the ERC Advanced grant DALDECS is acknowledged.

References

[1] Bachalo W 1980 Method for measuring the size and velocity of spheres by dual-beam light-scatter interferometry *Appl. Opt.* **19** 363–70

[2] Wigley G, Goodwin M, Pitcher G and Blondel D 2004 Imaging and PDA analysis of a GDI spray in the near-nozzle region *Exp. Fluids* **36** 565–74

[3] Cornillault J 1972 Particle size analyzer *Appl. Opt.* **11** 265–8

[4] Yeh C-N, Kosaka H and Kamimoto T 1993 A fluorescence/scattering imaging technique for instantaneous 2-D measurement of particle size distribution in a transient spray *Proc. 3rd Int. Congress on Optical Particle Sizing* pp 355–61

[5] Domann R and Hardalupas Y 2003 Quantitative measurement of planar droplet Sauter mean diameter in sprays using planar droplet sizing *Part. Part. Syst. Charact.* **20** 209–18

[6] Glover A, Skippon S and Boyle R 1995 Interferometric laser imaging for droplet sizing: a method for droplet-size measurement in sparse spray systems *Appl. Opt.* **34** 8409–21

[7] Maeda M, Kawaguchi T and Hishida K 2000 Novel interferometric measurement of size and velocity distributions of spherical particles in fluid flows *Meas. Sci. Technol.* **11** L13–8

[8] Malarski A and Leipertz A 2008 Dependence of the stimulated Raman scattering threshold in droplets on the temporal stretching of a nanosecond laser pulse *J. Raman Spectrosc.* **39** 700–6

[9] Braeuer A, Engel S R, Hankel R F and Leipertz A 2009 Gas mixing analysis by simultaneous Raman imaging and particle image velocimetry *Opt. Lett.* **34** 3122–4

[10] Hofeldt D L 1993 Full-field measurements of particle size distributions: II. Experimental comparison of the polarization ratio and scattered intensity methods *Appl. Opt.* **32** 7559–67

[11] Labs J E and Parker T E 2005 Multiple-scattering effects on infrared scattering measurements used to characterize droplet size and volume fraction distributions in diesel sprays *Appl. Opt.* **44** 6049–57

[12] Hertz H and Aldén M 1987 Calibration of imaging laser-induced fluorescence measurements in highly absorbing flames *Appl. Phys.* B **42** 97–102

[13] Versluis M, Georgiev N, Martinsson L, Aldén M and Kroll S 1997 2-D absolute OH concentration profiles in atmospheric flames using planar LIF in a bi-directional laser beam configuration *Appl. Phys.* B **65** 411–7

[14] Talley D G, Verdieck J F, McDonell V G, Lee S W and Samuelsen G S 1996 Accounting for laser sheet extinction in applying PLLIF to sprays *Proc. AIAA 34th Aerospace Sciences Meeting and Exhibit* AIAA 96-0469

[15] Abu-Gharbieh R, Persson J, Forsth M, Rosen A, Karlstrom A and Gustavsson T 2000 Compensation method for attenuated planar laser images of optically dense sprays *Appl. Opt.* **39** 1260–7

[16] Sick V and Stojkovic B 2001 Attenuation effects on imaging diagnostics of hollow-cone sprays *Appl. Opt.* **40** 2435–42

[17] Koh H, Jeon J, Kim D, Yoon Y and Koo J 2003 Analysis of signal attenuation for quantification of a planar imaging technique *Meas. Sci. Technol.* **14** 1829–38

[18] Koh H, Jung K, Yoon Y, Lee K and Jeong K 2006 Development of quantitative measurement of fuel mass distribution using planar imaging technique *J. Vis.* **9** 161–70

[19] Kalt P A M, Birzer C H and Nathan G J 2007 Corrections to facilitate planar imaging of particle concentration in particle-laden flows using Mie scattering: part 1. Collimated laser sheets *Appl. Opt.* **46** 5823–34

[20] Berrocal E, Churmakov D Y, Romanov V P, Jermy M C and Meglinski I V 2005 Crossed source-detector geometry for a novel spray diagnostic: Monte Carlo simulation and analytical results *Appl. Opt.* **44** 2519–29

[21] Berrocal E, Meglinski I and Jermy M 2005 New model for light propagation in highly inhomogeneous polydisperse turbid media with applications in spray diagnostics *Opt. Express* **13** 9181–95

[22] Brown C T, McDonell V G and Talley D G 2002 Accounting for laser extinction, signal attenuation, and secondary emission while performing optical patternation in a single plane *Proc. ILASS Americas 15th Ann. Conf. on Liquid Atomization and Spray Systems* pp 195–9

[23] Talley D G 2004 Optical patternation method *US Patent No* 6734965
[24] Koh H, Kim D, Shin S and Yoon Y 2006 Spray characterization in high pressure environment using optical line patternator *Meas. Sci. Technol.* **17** 2159–67
[25] Berrocal E, Kristensson E, Richter M, Linne M A and Aldén M 2008 Application of structured illumination for multiple scattering suppression in planar laser imaging of dense sprays *Opt. Express* **16** 17870–81
[26] Kristensson E, Berrocal E, Richter M and Aldén M 2010 Nanosecond structured laser illumination planar imaging for single-shot imaging of dense sprays *Atomization Sprays* **20** 337–43
[27] Keller P J, Schmidt A D, Santella A, Khairy K, Bao Z, Wittbrodt J and Stelzer E H K 2010 Fast, high-contrast imaging of animal development with scanned light sheet-based structured-illumination microscopy *Nature Methods* **7** 637–42
[28] Kristensson E, Araneo L, Berrocal E, Manin J, Richter M, Aldén M and Linne M 2011 Analysis of multiple scattering suppression using structured laser illumination planar imaging in scattering and fluorescing media *Opt. Express* **19** 13647–63
[29] Kristensson E, Berrocal E and Aldén M 2011 Extinction coefficient imaging of turbid media using dual structured laser illumination planar imaging *Opt. Lett.* **36** 1656–8
[30] Berrocal E, Kristensson E, Sedarsky D and Linne M 2009 Analysis of the SLIPI technique for multiple suppression in planar imaging of fuel spays *Proc. ICLASS 11th Triennial Int. Annual Conf. on Liquid Atomization an Spray Systems* p 469
[31] Berrocal E, Sedarsky D, Paciaroni M E, Meglinski I V and Linne M A 2009 Laser light scattering in turbid media: part II. Spatial and temporal analysis of individual scattering orders via Monte Carlo simulation *Opt. Express* **17** 13792–809